Contact epitaxy by deposition of Cu, Ag, Au, Pt, and Ni nanoclusters on (100) surfaces: Size limits and mechanisms

T. T. Järvi,* A. Kuronen, K. Meinander, and K. Nordlund
Accelerator Laboratory, University of Helsinki, P.O. Box 43, FI-00014 Helsinki, Finland

K. Albe
Institut für Materialwissenschaft, Technische Universität Darmstadt, Petersenstrasse 23, D-64287 Darmstadt, Germany
(Received 7 March 2006; revised manuscript received 17 January 2007; published 26 March 2007)

Low-energy deposition of individual metal clusters (6–2000 atoms) on a (100) surface is studied for copper, nickel, platinum, silver, and gold by means of molecular-dynamics simulations. For different temperatures ranging from 0 to 750 K we determine the maximum size of clusters that will achieve complete contact epitaxy upon deposition. The results show that two mechanisms contribute to epitaxial alignment. For the smallest cluster sizes, the heat of adsorption released at the interface will immediately (ps time scales) allow the cluster to melt and become epitaxial by resolidification. This effect gives roughly the same limit for all elements studied. On longer (ns) time scales, the clusters can align epitaxially by thermally actived motion of twinning dislocations. This mechanism leads to much higher limits of epitaxy than the resolidification process. Moreover, the resulting limits differ significantly between the elements.

DOI: 10.1103/PhysRevB.75.115422 PACS number(s): 61.46.Df, 61.72.Mm, 61.72.Lk, 64.70.Nd

I. INTRODUCTION

Thin films are widely used in contemporary science and technology since they can improve the mechanical, optical, electronic, and magnetic properties of materials.[1] If the thin-film deposition shall cause no or very little damage to the substrate, nanocluster deposition at low energies can be an alternative to conventional deposition methods, because it allows significant growth rates at low deposition rates.[2] Since the cluster size offers one more degree of freedom in the deposition conditions, nanocluster deposition allows access to process windows (defined by, e.g., incoming particle energy, substrate temperature, etc.) that do not exist for conventional deposition methods. Moreover, nanocluster deposition offers a natural way to grow nanocrystalline thin films with a well-controlled grain size.

Cluster deposition methods differ from single-atom ones in that a cluster incoming on a substrate has an internal atomic structure, which is randomly oriented with respect to the substrate. The first step in the development of nanocluster growth methods for single-crystalline substrates is thus to understand under which conditions the deposited clusters become epitaxial with the substrate. If they always become epitaxial immediately on impact (before the next cluster lands in the same position), the deposition results in epitaxial growth. If all or parts of the cluster remain in a random orientation, nanocrystalline growth will result.

At high enough deposition energy it is always possible to get epitaxial clusters. However, high energies damage the substrate upon which the clusters are deposited, and hence there has been considerable interest in studying low-energy cluster beam deposition. Several studies have noted that when low-energy clusters are deposited on a surface, smaller clusters tend to align epitaxially, while larger ones retain some part of their original structure.[3–7] This is usually attributed to, e.g., competition between the adsorption energy released in the impact and the intrinsic stress energy of the cluster,[4,8] or, in the case of the cluster and substrate consisting of different elements, to the relative hardness of the cluster and substrate.[4] For face-centered-cubic (fcc) metals the boundaries between epitaxial and nonepitaxial parts have been reported to be twin boundaries,[5,9] which is natural since the twin boundary energy in fcc metals is very low.[10] The consequences of this fact have, however, not been studied in detail so far, and there is, to our knowledge, no study that has systematically examined the boundary between epitaxial and nanocrystalline growth.

In a previous work from our group,[11,12] the maximum copper cluster size for which epitaxial growth can be achieved for deposition on a copper (100) surface was determined using molecular-dynamics simulations. It was found that the effective radius of the limiting cluster size is roughly linearly proportional to temperature, in the temperature range 0–750 K.

The aim of the current work is to use a comparison between different elements to be able to correlate material parameters with the degree of epitaxy, and thus determine the mechanism by which epitaxy is achieved for single clusters. This is the first step towards understanding thin-film growth; although on continued deposition also surface roughness[13,14] and adatom migration[15] affect the final state, knowing the mechanism by which the first clusters become (or do not become) epitaxial is crucial for understanding all the further steps.

II. METHOD AND SIMULATIONS

We examined the limiting size of clusters that achieve complete epitaxy upon deposition on a (100) surface using molecular-dynamics simulations. The limit was determined for copper, nickel, platinum, silver, and gold, in the temperature range 0–750 K, the surface and cluster always being at the same temperature and consisting of the same element.

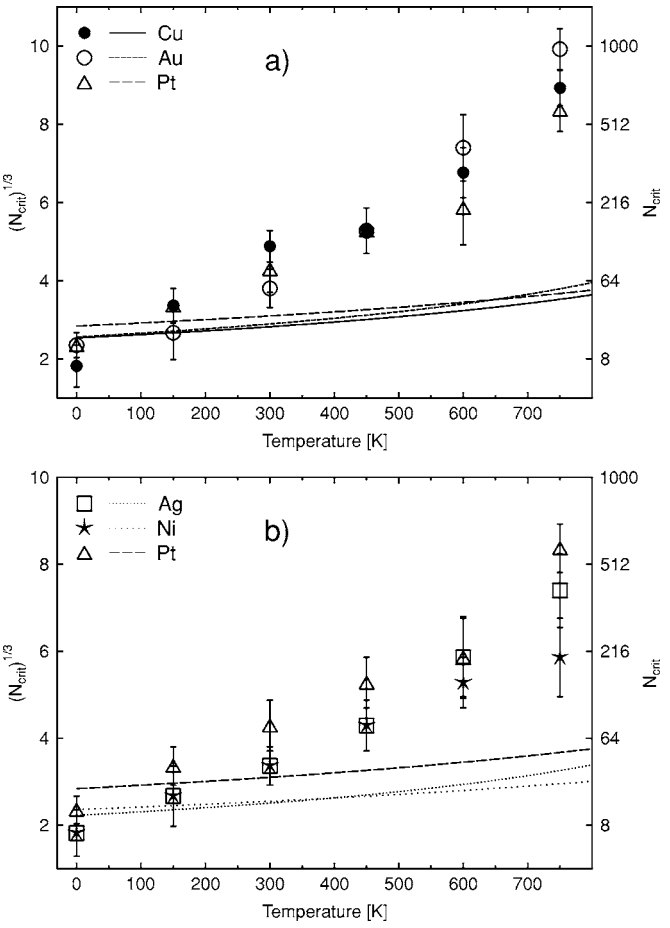

FIG. 1. Maximum size, N_{crit} (i.e., number of atoms), of clusters that align completely epitaxially upon deposition. The upper error limits show the smallest nonepitaxial cluster sizes. The curves show the predictions of the model presented in Sec. III A. The model takes only cluster heating into account. The figure is split into two parts for clarity, each part showing three of the five elements.

The embedded-atom-method potentials[16] by Foiles *et al.*[17] were used to describe the interatomic interactions. These potentials are widely tested and have a common parametrization. They have been fitted to the same properties of the corresponding elements, that is, to the lattice constant, sublimation energy, bulk modulus, elastic constants, and vacancy formation energy. In addition, an analytic bond-order potential for platinum[18] was used since it reproduces the high experimental stacking fault energy. This potential will be referred to as Pt_{BO}.

It must be emphasized that none of the potentials reproduce the properties of the corresponding element perfectly. Therefore the elements must be regarded as a representative set of fcc metals, rather than their exact counterparts in nature.

The simulation procedure was as follows. The clusters were created as cuboctahedra and relaxed for 25 ps while keeping the temperature constant using the temperature control algorithm by Berendsen *et al.*[19] After this, the clusters were allowed to float freely for 2 ns to make sure they had reached stable minima. Only in the cases of the softer elements (as measured by the Debye temperature, i.e., Ag, Au, and Pt) and temperatures above 450 K was there any further evolution during the free float, indicated by a rise in temperature. In these cases the temperature control and free float were repeated until a stable configuration had been obtained. At all temperatures, most clusters remained cuboctahedra upon relaxation. The ones with atom numbers equal to one of the icosahedral magic numbers[20] invariably relaxed to multiply twinned icosahedra. Note that in a previous study by our group,[11,12] the effect of the initial cluster morphology on epitaxial alignment was shown to be minor.

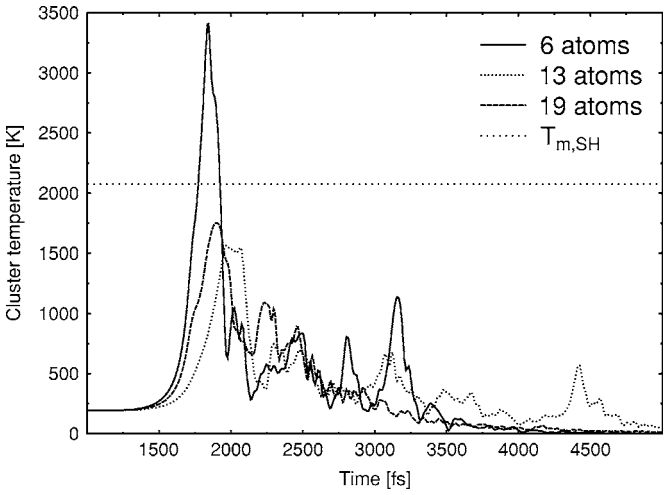

FIG. 2. Temperature profile of nickel clusters at 0 K. The horizontal line shows the mechanical melting point. The cluster with six atoms becomes epitaxial, the larger ones do not.

The deposited clusters varied in size from 6 to ~2000 atoms and the (100) surface area was chosen such that its lateral size was at least three times the cluster diameter. Periodic boundary conditions were applied in the (010) and (001) directions. In addition, two atomic layers at the sides and bottom of the cell were kept at the chosen temperature, and two further layers were fixed at the bottom of the cell to simulate bulk matter.

After relaxing both the cluster and surface, the cluster was rotated randomly and placed above the surface. It was translated randomly from the center of the surface in the interval $[-a,a]$ in both the (010) and (001) directions, where a is the lattice constant at the temperature in question. In the (100) direction the cluster was placed just beyond the potential cutoff from the top surface atoms. A kinetic energy of 25 meV per atom was then given to the cluster towards the surface and the simulation was run for 2 ns. This deposition energy is small enough not to play any role in epitaxial alignment.

For each cluster size and temperature, 20 simulations were run to collect statistics. This number is rather small, but compensated by the fact that the number of nonepitaxial final states rises fast with the number of atoms, such that the limit of epitaxy can be determined reliably.

To find the maximum size of clusters that would align completely epitaxially with the surface, we chose (arbitrarily) to consider a particular cluster size epitaxial, if less than one tenth of the simulated events were nonepitaxial,

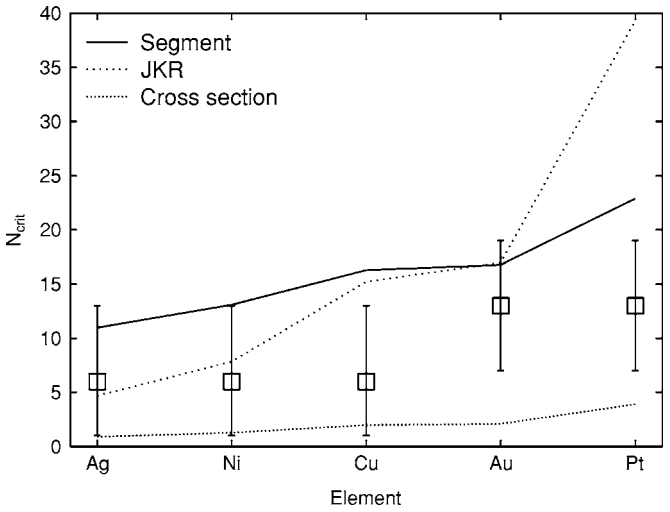

FIG. 3. Critical cluster sizes at 0 K predicted by different mechanical melting models. In "Segment" and "Cross section" the surface areas lost due to the adsorption are $2\pi rh$ and πr^2, respectively. In "JKR" the area is determined by the model of Johnson, Kendall, and Roberts (see text). The markers show the sizes obtained from simulation.

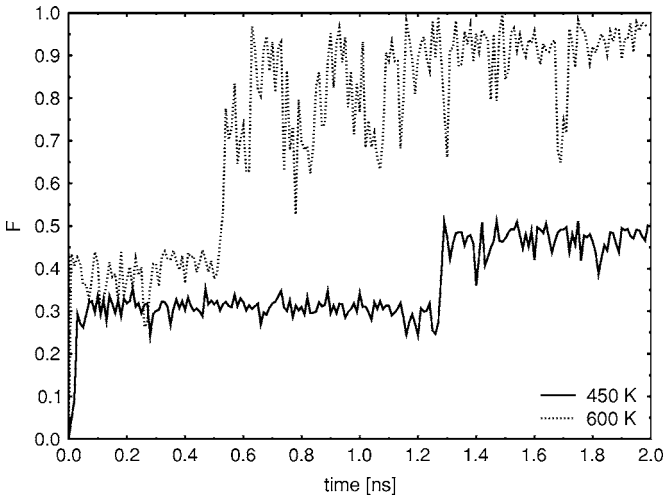

FIG. 4. Time evolution of the normalized structure factor with Miller indices (1,1,1) in two simulations of Ni clusters, one of 147 atoms at 600 K, the other of 405 atoms at 450 K.

corresponding to a 90% confidence interval. Each individual cluster was judged epitaxial if there were no stable twins or other grain boundaries within the cluster during the 2-ns simulation. Hence clusters in which planar defects appeared and disappeared were considered epitaxial even if the final state had a subgrain. Epitaxiality was thus determined mainly by visual inspection.

As a quantitative measure of the degree of epitaxy,[9] we calculated the structure factor

$$S = \frac{1}{N}\sum_{i=1}^{N} e^{i\mathbf{k}\cdot\mathbf{r}_i}, \tag{1}$$

where the sum is over the N atoms, with coordinates $\mathbf{r}_i$, in the system, and k is the wave vector

$$\mathbf{k} = \frac{2\pi}{a}(n_1, n_2, n_3) \tag{2}$$

with the Miller indices n_i and lattice constant a. The square of the structure factor calculated from the cluster atoms was normalized to the structure factor of the substrate. Thus defining

$$F = \frac{|S_{\text{cluster}}|^2}{|S_{\text{substrate}}|^2}, \tag{3}$$

a value close to unity indicates epitaxy. However, the structure factor unfortunately does not admit easy comparison between elements. This is due to the differences in their thermal vibrations.

III. RESULTS

Results for the maximum size N_{crit} of clusters that reach complete epitaxy upon deposition on a surface are shown in Fig. 1. The left vertical axis shows the cube root of the number of cluster atoms which serves as an effective radius for the clusters. The upper error limit shows the next largest cluster size, which no longer is epitaxial. Thus the error bars are not defined in a statistical sense and it must be emphasized that the ordering of the critical cluster sizes between the elements is significant at the high temperatures.

The upper cluster size limit for complete epitaxy has been previously determined for the case of copper in Refs. 11 and 12. Our present results for Cu agree with the ones presented there. The roughly linear dependence between the effective radius of the limiting cluster size and the temperature, observed in Refs. 11 and 12, equally holds true for the elements studied in this work.

Apart from the overall increase of the limit of epitaxy with temperature, there are two main features. We will first discuss the low- and then the high-temperature behavior of the limit.

A. Low temperature: Cluster heating

First, at low temperatures ($\lesssim$150 K), the limit of epitaxy is relatively independent of element. Here the limit is low, corresponding to a cluster of at most $\sim$100 atoms. Visual inspection showed that in these cases the epitaxial configu-

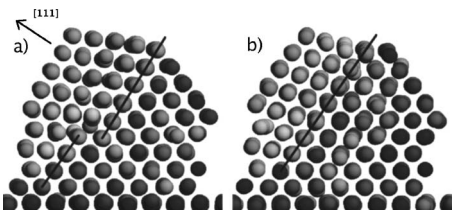

FIG. 5. Kinked twin boundary, indicated by a line, in a 405-atom Ni cluster at 450 K. The two parts show the cluster (a) before and (b) after the transition detailed in Sec. III C. In both cases, the nonepitaxial part of the cluster can be seen to the left of the twin boundary.

TABLE I. Barriers $\gamma_{UTB}-\gamma_{TB}$ for twin boundary migration and the main elemental properties of the Foiles potentials (Ref. 17), as well as the bond-order potential for Pt (Ref. 18), used in the present study. The properties are the mechanical melting point $T_{\mathrm{melt}}^{\mathrm{SH}}$, the (100) surface energy $\gamma_{\{100\}}$, and the twin boundary energy γ_{TB}. The experimental values are from Ref. 10.

	Ni	Ag	Pt	Cu	Au	Pt_{BO}
$T_{\mathrm{melt}}^{\mathrm{SH}}/\mathrm{K}$	2075	1405	1865	1555	1380	3265
$\gamma_{\{100\}}/\frac{J}{m^2}$	1.57	0.70	1.65	1.29	0.91	1.71
$\gamma_{TB}/\frac{mJ}{m^2}$	7.23	0.74	7.32	8.85	2.37	166
$\gamma_{TB}/\frac{mJ}{m^2}$ (expt.)	43	8	161	24	15	161
$\gamma_{UTB}-\gamma_{TB}/\frac{mJ}{m^2}$	219	118	129	133	99	423

ration was usually achieved on short (below ~50 ps) time scales, if it was achieved at all during the whole 2-ns simulation. This can be understood by monitoring the temperature profile which shows that the cluster is raised to a high temperature on impact, as the surface energies at the cluster-substrate interface are released. The temperature profiles in the case of nickel clusters at 0-K initial temperature are shown in Fig. 2. The heating allows for complete reordering of the cluster, as observed in previous works.[4,9,11,12,21]

What is somewhat surprising in our results is that this effect appears to be independent of element within the uncertainty. This can be understood by calculating the size of the largest cluster that melts upon deposition. A melting temperature independent of cluster size is used in the calculation. We return to the motivation of this approach later.

As the cluster lands on the surface, the energy release, and thus cluster heating, is as a first approximation proportional to the surface energies, according to

$$\Delta E = \frac{2\gamma A}{\beta}, \tag{4}$$

where γ is the surface energy and $2A$ the surface area lost due to the adsorption. β is inserted to account for a possible difference in the amount of energy transferred to the cluster and to the substrate. We set $\beta=2$, corresponding to half the energy to the cluster and half to the substrate. The difference in the result caused by a different β is qualitatively negligible.

There are several possible ways to define the contact area A between the cluster and substrate. For the time being, we approximate the cluster by a sphere and estimate A by the area of its segment, with height h, so that $A=2\pi rh$, where r is the radius of the cluster. Cluster atoms close enough to the substrate, i.e., within the interaction range, can be regarded as taking part in the cluster-substrate interface. Hence h will be taken equal to one lattice constant, i.e., $h=a$, which is almost exactly equal to the interaction range of the potential. Other possible definitions of A will be discussed below.

The change in temperature needed to melt a cluster is $\Delta T=T_{\mathrm{melt}}-T_i$, where T_i is the cluster's initial temperature. Setting the energy required for this heating equal to the surface energy released to the cluster gives the relation

$$\frac{3}{2}Nk_B\Delta T = \frac{\Delta E}{2}, \tag{5}$$

where N is the number of atoms in the cluster, $N=\frac{16\pi r^3}{3a^3}$. The released energy is divided by 2 due to the equipartition theorem. We thus have for the limiting cluster size the expression

$$r_{\mathrm{crit}} = \sqrt{\frac{\gamma h a^3}{4k_B\beta}}\frac{1}{\sqrt{T_{\mathrm{melt}}-T_i}}. \tag{6}$$

As mentioned earlier, the above derivation has been made assuming a melting temperature independent of cluster size, whereas it is well known that the melting of nanoclusters is a subtle issue.[20] However, in the case of cluster deposition, the heating induced by the released surface energy dissipates very fast, within a few ps. Hence thermodynamic melting, which is a nucleation-and-growth process, can be questioned as the relevant mechanism. Instead, we propose that in order for the cluster to melt, the temperature has to rise above the mechanical melting point, or the limit of superheating.[22–26] At this temperature, the *local* free-energy minimum at the solid phase disappears, allowing for an immediate melting and subsequent recrystallization. Furthermore, as mechanical melting is homogeneous, it can be assumed to be independent of cluster size. Also, for the thermodynamic melting temperature of clusters of less than 100 atoms, no analytic formula exists, and the melting point does not vary smoothly with cluster size.[20] Finally, note that the mechanical melting temperature is about 15–20 % above the bulk thermodynamic melting temperature for a wide range of materials.[24–26]

The curves calculated with Eq. (6) are shown in Fig. 1 together with the simulation results. The curves have been calculated with the mechanical melting points, or temperature limits of superheating $T_{\mathrm{melt}}^{\mathrm{SH}}$, {100} surface energies $\gamma_{\{100\}}$, and lattice constants a, obtained from the corresponding potentials. The first two of the above quantities are listed in Table I. The mechanical melting points were obtained by simulating a small crystalline cell with periodic boundary

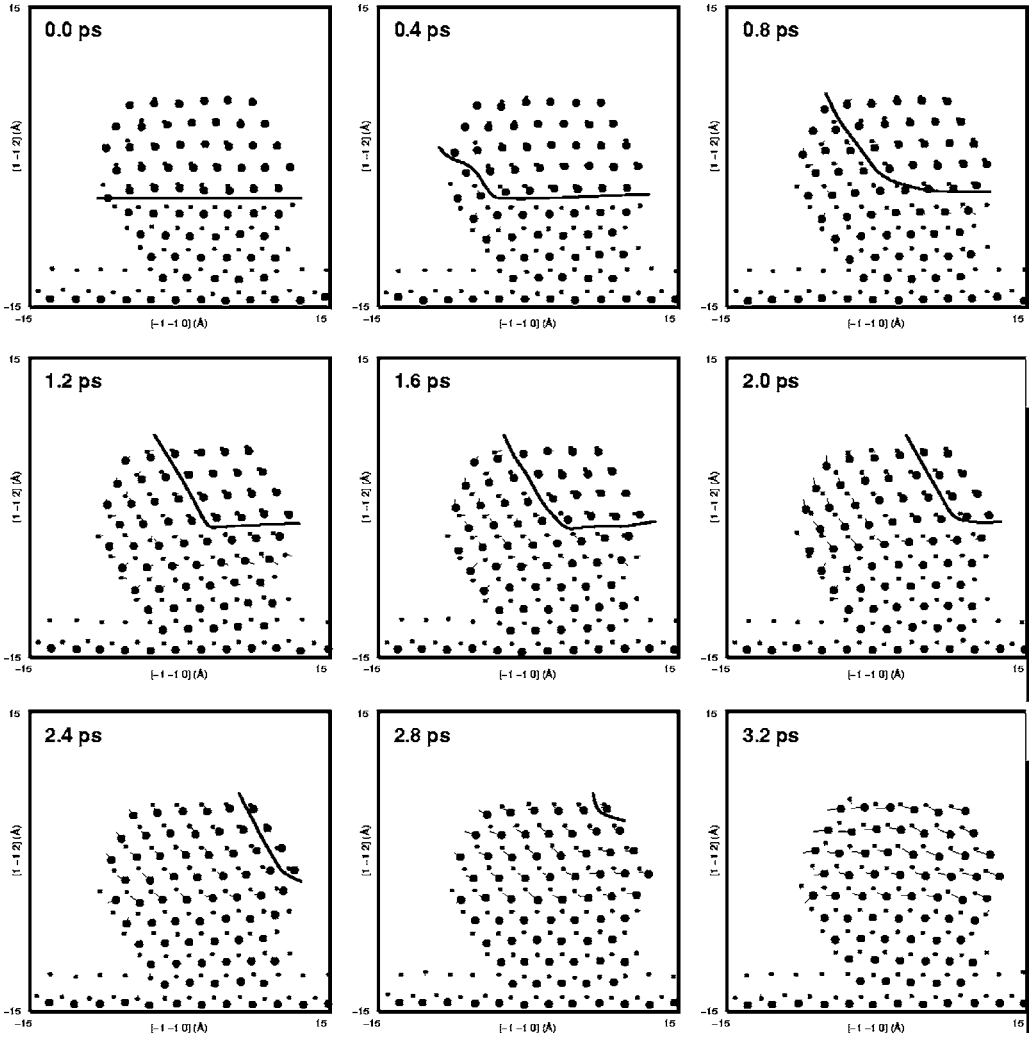

FIG. 6. A change in the stacking of a 405-atom Ni cluster (shown in Fig. 5) where a twin boundary moves one layer towards the surface. The large spheres represent the fourth and the small spheres the sixth {111} layer (see text). For every frame, the spheres indicate the atom positions at the given time while the lines give their movement since the first frame. The Shockley partial dislocation line is sketched in each frame.

conditions and pressure control, (hence allowing for no nucleation centers for equilibrium melting) and determining the temperature at which the crystal melted.

The above calculation gives good agreement with the limit of epitaxy at low temperature, and the different elements have, according to the model, very similar limits throughout the current temperature scale.

To repeat, the main assumptions in our model are (i) the size independence of the mechanical melting point and (ii) the choice of the definition of A. To examine other choices for A, we consider two more cases. First, for very small clusters, simply the cluster cross section $A=\pi r^2$ could be considered, giving $r_{\mathrm{crit}} \propto (T_{\mathrm{melt}}-T_i)^{-1}$. Second, we could take the Hertz contact law.[27,28] The model of Johnson, Kendall, and Roberts[28,29] (JKR) modifies this to include an adhesive force resulting from the surface energy $U=-\pi r_c^2 2\gamma$, where r_c is the radius of the interface region. This model results in a critical cluster size

$$r_{\mathrm{crit}} = \left(\frac{\gamma C^{\mathrm{JKR}} a^3}{8\pi k_B \beta (T_{\mathrm{melt}} - T_i)} \right)^{3/5}. \tag{7}$$

The constant $C^{\mathrm{JKR}}=\pi[18\pi\gamma(1-\nu^2)/Y]^{2/3}$, where Y and ν are the (in this case microscopic) Young's modulus and Poisson's ratio[17] of the material, respectively. The results at 0 K from the melting model with the above definitions of A are shown in Fig. 3. From the figure, it seems that our simulations are not accurate enough to make a difference between the different possible choices for the contact area. The segment based model and the JKR model seem to be somewhat better than the cross-section based model, except for the prediction of the JKR model for platinum.

The decisive role of the mechanical melting point can also be seen from the temperature profiles, shown for nickel clusters at 0 K in Fig. 2. The largest epitaxial cluster size is six atoms, which is also the largest size for which the temperature reaches above the mechanical melting point. Similar behavior is observed for the other elements.

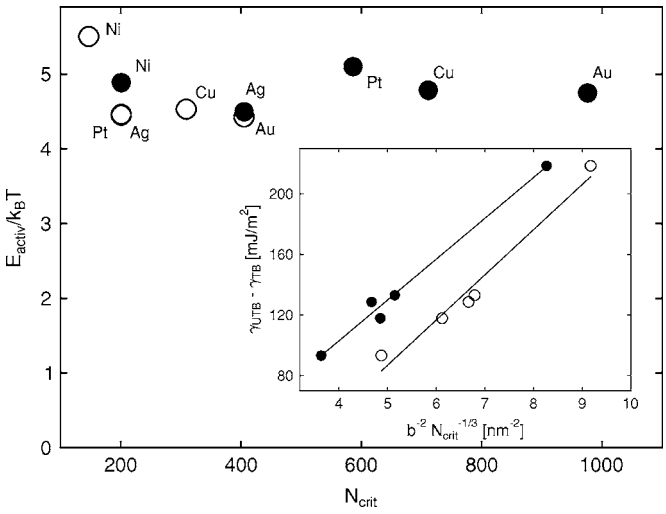

FIG. 7. Activation energy for thermal motion of twinning dislocations over k_BT in various metal clusters of critical size N_{crit} at 750 K (filled circles) and 600 K (empty circles). The activation energies are close to 0.31 and 0.23 eV at 750 and 600 K, respectively. The inset shows the linear correlation between the barrier $\gamma_{UTB}-\gamma_{TB}$ and the critical cluster size.

The fact that the limits at low temperature are so close to each other can now be understood. Note the surface energies which are listed in Table I. These differ by at most about a factor of 2, but the elements with the highest surface energies (Ni and Pt) also have the highest melting points (30–50 % higher than that of Ag, which has the lowest surface energy). Hence the elements with the highest energy release are also the ones where it is hardest to melt the cluster and cause reordering of it. Since these two effects thus counteract each other, the expected difference in the simulated limit of epitaxy is comparable to the uncertainty, and thus not visible in our results.

Finally, as the melting model dominates only below ~150 K for the present results, we used an analytic bond-order potential for platinum,[18] for which the melting model dominates over the entire temperature range, to further assess the model. We will return to this in Sec. III E after describing the high-temperature behavior of the limit of epitaxy.

B. High temperature

We now discuss the high-temperature (≳600 K) behavior of the limit of epitaxy. Here the differences between the elements grow until, at the highest temperature 750 K, there is a difference of a factor of roughly 5 between the lowest and highest limit of epitaxy. This difference cannot be understood in terms of the cluster heating. First, the limits are much larger than predicted by the model described before. Moreover, both visual inspection and systematic analysis of the results showed that epitaxial alignment occurs at time scales beyond the picosecond range (when the initial heating occurs). This is clearly visible from the evolution of the normalized structure factor presented in Eq. (3). The structure factor is shown in Fig. 4 in the cases of two nickel clusters. In both cases there is a late epitaxial alignment occurring after several hundred picoseconds. We next analyze in detail the mechanism of epitaxial alignment at the highest temperatures.

C. Atom-level mechanism: A case study

As a cluster is deposited on the surface, there is an initial period of disorder after which the cluster recrystallizes epitaxially either partly or in whole. In the case of partial epitaxy, the vast majority of nonepitaxial grains are accomodated to the epitaxial part with {111} twin boundaries, as noted before.[5,9] Such a boundary is shown in Fig. 5 in the case of a 405-atom Ni cluster at 450 K.

The appearance of twin boundaries is not surprising, since their energy is very low, from about one-tenth to one-thousandth of the surface energy. The twin boundary energies γ_{TB}, evaluated with the potentials used in the present study, are shown in Table I with experimental values.[10] The dominance of {111} twin boundaries as the interfaces separating the epitaxial and nonepitaxial parts of deposited clusters hints that the limit of epitaxy may be determined by the mobility of these boundaries.

A typical change in stacking where a twin boundary moves one layer towards the surface is shown in Figs. 5 and 6. Parts (a) and (b) of Fig. 5 show the cluster before and after the transition, respectively.

Figure 6 shows the fourth and sixth {111} layers of the cluster, counting from the upper left surface in Fig. 5. That is, the line of sight is antiparallel to the [111] direction in Fig. 5 and the layers shown are the ones on both sides of the twin boundary in part (a).

In the first frame of Fig. 6 the stacking, counting from the seventh layer to the surface, is A**BC**B**A**CB, where the layers shown in the figure have been emphasized. Thus there is a twin boundary and a total of four layers are nonepitaxial. During about 3 ps, a twinning dislocation moves through the cluster changing the stacking in such a way that the first nonepitaxial layer (the fourth one) becomes epitaxial. The rest of the nonepitaxial layers also glide in the same direction.

The dislocation is a Shockley partial,[10] which is located in the kink of the initial twin plane. The dislocation line is illustrated in Fig. 6. Due to thermal activation, the dislocation surmounts a barrier and glides through the cluster leaving behind a perfect fcc lattice.

After the transition the stacking is A**BC**A**C**BA. That is, the twin boundary has moved by one layer, as shown in part (b) of Fig. 5. The transition can be seen as a sudden jump in the normalized structure factor, shown as the 450-K line in Fig. 4.

D. Activation energies

The activation energy of a twinning dislocation to move over the Peierls barrier is determined by the difference between the stable and unstable twinning fault positions, since the moving partial dislocation introduces a local stacking fault.[10] Hence the relevant barrier is $\gamma_{UTB}-\gamma_{TB}$, γ_{TB} being the twin boundary energy and γ_{UTB} the energy at the unstable

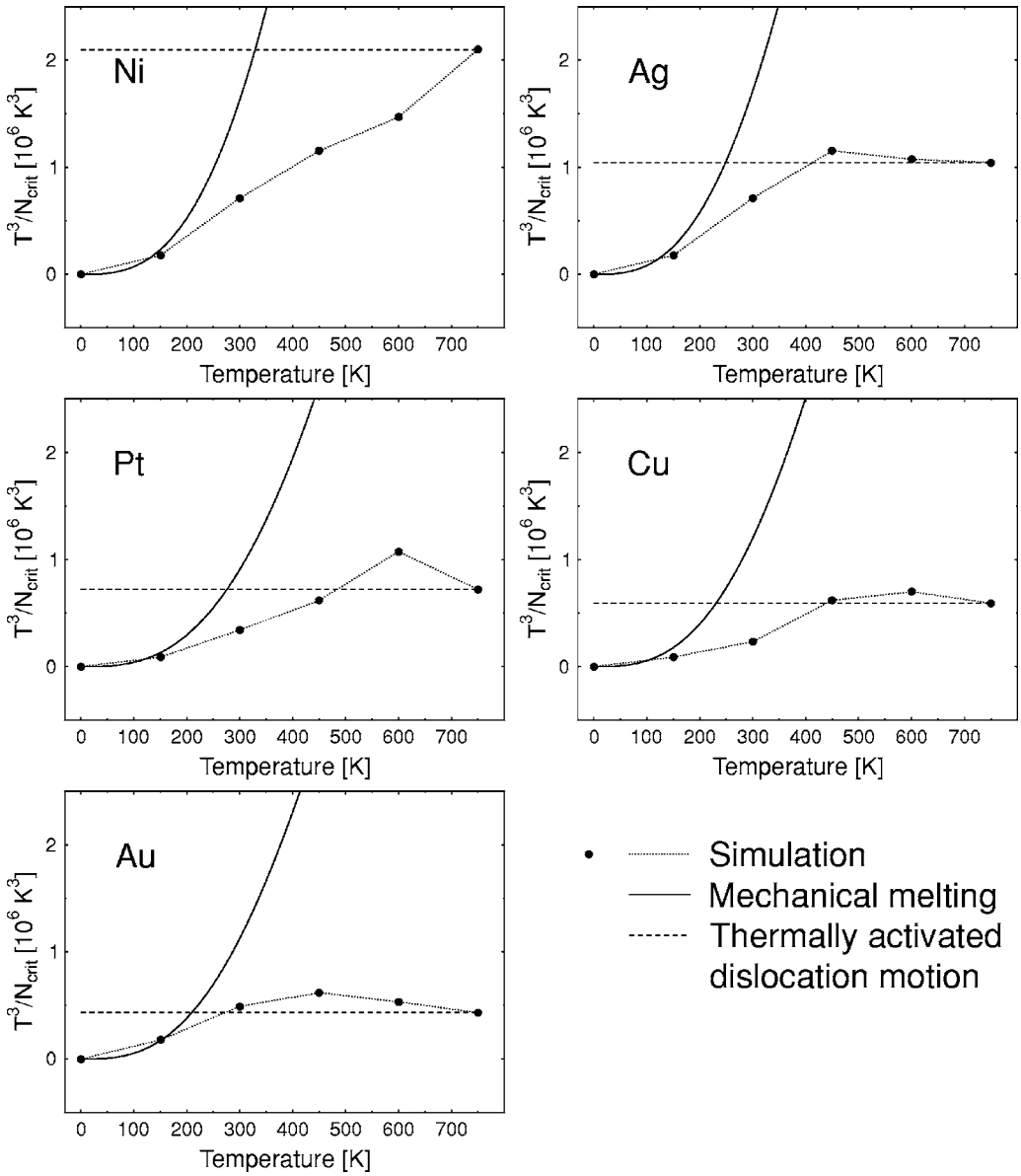

FIG. 8. The fraction $\frac{T^3}{N_{\text{crit}}}$ as a function of temperature for the five elements. The horizontal lines show the constants implied by the thermally activated process and simulation at 750 K. The curves give the predictions of the melting model of Sec. III A.

twinning fault position. The values for the present potentials[33] are listed in Table I.

The energy barrier, or activation energy, E_{activ}, which a dislocation line of length l has to overcome when it moves a distance of $b=\frac{a}{\sqrt{6}}$ into the next minimum position is thus

$$E_{\text{activ}} = (\gamma_{UTB} - \gamma_{TB})bl. \tag{8}$$

We now assume that stacking fault energies are not significantly changed by finite-size effects and that the Peierls barrier estimated for the bulk material is about the same in a nanoparticle. A sensible measure for the length of the dislocation line is the diameter l of the cluster, which, for a spherical object, is given by

$$l = 2r = 2\left(\frac{3}{4\pi\rho}N\right)^{1/3}, \tag{9}$$

where ρ is the atomic volume density and N is the number of atoms in the cluster. With this relation the activation energy E_{activ} becomes a function of cluster size N.

Let Γ be the frequency for a twinning dislocation of length l to cross the Peierls barrier. According to transition state theory, the temperature dependence should then be given by

$$\Gamma = \Gamma_o \exp^{-E_{\text{activ}}/k_B T}, \tag{10}$$

where the prefactor describes the total number of attempts, which can be approximated by $\Gamma_o \propto \nu_D l$. Here ν_D is the Debye frequency and l, the cluster diameter, is proportional to

the number of sites at which the dislocation can start to move. Our simulations reveal, as shown in Sec. III C and Fig. 6, that after the thermally activated dislocation motion has begun, the dislocation line is dragged to the surface by athermal processes, most likely by increasing image forces. When the dislocation line has reached the surface, it is annealed and the twinning plane has been displaced by one lattice spacing $d_{\{111\}}$. In order for the particle to become fully epitaxial about $n=r/d_{\{111\}}$ thermally activated processes are necessary. For a given total simulation time t (now 2 ns) we finally obtain the expression

$$n = \frac{r}{d_{\{111\}}} \propto t\nu_D l \exp^{-E_{\text{activ}}(N_{\text{crit}})/k_B T}, \tag{11}$$

where it must be emphasized that the activation energy is evaluated at the critical cluster size.

With Eq. (9) the geometry factors l and r cancel and it follows that

$$t\exp^{-E_{\text{activ}}(N_{\text{crit}})/k_B T} \propto \frac{1}{d_{\{111\}}\nu_D} \approx \text{const} \tag{12}$$

for the critical cluster sizes N_{crit}. The factor $1/d_{\{111\}}\nu_D$ is constant within 34%, or 26% if the value for nickel, which deviates the most from the thermally activated behavior due to its high barrier, is excluded.

Indeed, if we now take the critical cluster sizes N_{crit} of the various elements at a given temperature (750 K) and calculate the corresponding activation energies from Eq. (8), we find about the same value close to 0.31 eV for all metals considered here (see Fig. 7). The same observation holds true for the next highest temperature (600 K), where the activation energy is again the same, about 0.23 eV, for all metals, with the only exception of Ni with an activation energy of 0.28 eV. This is because Ni is the element with the highest barrier for dislocation motion, and hence the one for which the mechanism is the weakest. Obviously, thermally activated motion of twinning dislocations is the dominant mechanism for epitaxial reorientation at high temperatures.

Comparison between the barrier and the results in Figs. 1 and 7 shows that the maximum size of epitaxial clusters at the higher temperatures correlates with $\gamma_{UTB}-\gamma_{TB}$ like

$$\gamma_{UTB} - \gamma_{TB} \propto \frac{1}{b^2 N_{\text{crit}}^{1/3}}, \tag{13}$$

which follows directly from Eqs. (8) and (9). This correlation is shown in the inset of Fig. 7.

E. Transition between heating and dislocation regimes

From the simulation results in Fig. 7 and Eq. (12) it follows that the ratio E_{activ}/T is constant in the temperature regime, where the dislocation mechanism is active. For a single element, this, together with Eqs. (8) and (9), implies that the fraction $\frac{T^3}{N_{\text{crit}}}$ is constant. Figure 8 shows the fraction $\frac{T^3}{N_{\text{crit}}}$ as a function of temperature for the five elements, together with the curves predicted by the cluster melting model presented in Sec. III A [Eq. (6)], and the constants implied by the simulations at 750 K. The transition from the low- to the high-temperature regime can clearly be seen. Only in the case of nickel, which has the highest barrier to dislocation motion, does the fraction $\frac{T^3}{N_{\text{crit}}}$ not become constant.

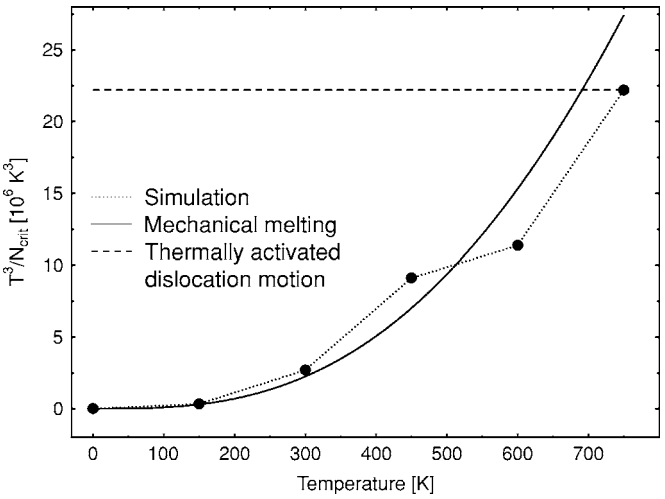

FIG. 9. The fraction $\frac{T^3}{N_{\text{crit}}}$ in the case of platinum with the bond-order potential (Ref. 18). The horizontal line shows the constant implied by the thermally activated process and simulation at 750 K. The curve gives the prediction of the melting model of Sec. III A.

If the activation barrier $\gamma_{UTB}-\gamma_{TB}$ becomes very high, the dislocation mechanism does not become active and mechanical melting is the dominant mechanism. In order to prove this statement and validate the melting model, we carried out additional simulations with an analytic bond-order potential for platinum,[18] which reproduces the high experimental stacking fault energy and gives a very high barrier to twin boundary migration, namely 423 mJ/m^2. This minimizes the effect of the dislocation mechanism described above. The potential's properties are summarized in Table I.

Repeating the analysis of the fraction $\frac{T^3}{N_{\text{crit}}}$ above for this potential gives the curves shown in Fig. 9. Obviously the mechanical melting model nicely describes the simulation results over the full temperature range, whereas the naive application of the dislocation model gives an entirely different behavior. (Note again that the mechanical melting model has no parameters fitted to the data.) Moreover, as the cluster sizes are so small (the largest epitaxial cluster size at 750 K is 19 atoms), it is questionable whether applying the dislocation model in this case would make sense anyway.

IV. DISCUSSION

Our results, showing the importance of dislocation activity in epitaxial alignment, are well in line with those of Ref. 30 where copper nanocluster sintering was studied using molecular-dynamics simulation. It was found that sintering occurs by a dislocation mechanism rather than local melting at the interface. The importance of dislocations in nanoparticle reactions was also shown in the case of Pt nanocluster rotation on Pt surfaces in Ref. 31.

Due to the thermally activated nature of the dislocation activity process, the limited time scales accessible to molecu-

lar dynamics may affect the results. It can therefore be expected that especially at the higher temperatures, the differences in the cluster size limit between the elements are underestimated by this study.

On the other hand, during multiple cluster deposition the roughness induced by previous clusters is expected to decrease the cluster size limit for complete epitaxy.[13,14] However, as stated in the introduction, the aim of the current work is to determine the mechanism by which clusters achieve epitaxy. The twin boundary movement mechanism recognized here can also be expected to be active during multiple cluster impacts.

V. CONCLUSIONS

We have determined the maximum size at which single clusters align completely epitaxially upon deposition on a (100) surface for the five fcc elements copper, silver, gold, nickel, and platinum, on a nanosecond time scale.

The limit of epitaxy is relatively independent of element at low temperatures. We explain this by calculating the maximum size of clusters that melt due to the surface energy released in the impact. The melting is understood in terms of mechanical melting. At high temperatures, we find that the clusters can align epitaxially by a dislocation glide mechanism, causing the migration of the {111} twin boundaries which separate the epitaxial and nonepitaxial parts of the clusters. This mechanism results in a much higher limit of epitaxy than would be possible due to the initial heating only. Moreover, the resulting limits differ significantly between the elements.

ACKNOWLEDGMENTS

This study was supported by the Academy of Finland, Project No. 205729 under the Center of Excellence in Computational Molecular Science. We also gratefully acknowledge the grants of computer time from CSC, the Finnish IT Centre for Science.

*Electronic address: tommi.t.jarvi@helsinki.fi

[1] J. A. Venables, *Introduction to Surface and Thin Film Processes* (Cambridge University Press, Cambridge, England, 2000).
[2] P. Jensen, Rev. Mod. Phys. **71**, 1695 (1999).
[3] M. Yeadon, J. C. Yang, M. Ghaly, R. S. Averback, and J. M. Gibson, Mater. Sci. Eng., B **67**, 76 (1999).
[4] Y. X. Wang, Z. Y. Pan, Y. K. Ho, Z. Huang, A. J. Du, Q. Wei, and Y. Xu, Surf. Coat. Technol. **158-159**, 258 (2002).
[5] S.-C. Lee, B. D. Yu, D.-Y. Kim, and N. M. Hwang, J. Cryst. Growth **242**, 463 (2002).
[6] A. Dzhurakhalov, A. Rasulov, T. V. Hoof, and M. Hou, Eur. Phys. J. D **31**, 53 (2004).
[7] H. Lei, Q. Hou, and M. Hou, Nucl. Instrum. Methods Phys. Res. B **164-165**, 537 (2000).
[8] L. Bardotti, B. Prével, P. Mélinon, A. Perez, Q. Hou, and M. Hou, Phys. Rev. B **62**, 2835 (2000).
[9] M. Hou, Nucl. Instrum. Methods Phys. Res. B **135**, 501 (1998).
[10] J. P. Hirth and J. Lothe, *Theory of Dislocations*, 2nd ed. (Krieger Publishing Company, Malabar, Florida, 1992).
[11] K. Meinander, J. Frantz, K. Nordlund, and J. Keinonen, Thin Solid Films **425**, 297 (2003).
[12] The temperature scale of Fig. 5 in Ref. 11 has to be rescaled by a factor of $\frac{36}{25}$.
[13] K. Meinander, K. Nordlund, and J. Keinonen, Nucl. Instrum. Methods Phys. Res. B **228**, 69 (2005).
[14] K. Meinander, T. T. Järvi, and K. Nordlund, Appl. Phys. Lett. **89**, 253109 (2006).
[15] J. Frantz, M. Rusanen, K. Nordlund, and I. T. Koponen, J. Phys.: Condens. Matter **16**, 2995 (2004).
[16] M. S. Daw and M. I. Baskes, Phys. Rev. B **29**, 6443 (1984).
[17] S. M. Foiles, M. I. Baskes, and M. S. Daw, Phys. Rev. B **33**, 7983 (1986).
[18] M. Müller, Ph.D thesis, Technische Universität Darmstadt, (2007).
[19] H. J. C. Berendsen, J. P. M. Postma, W. F. van Gunsteren, and J. R. Haak, J. Chem. Phys. **81**, 3684 (1984).
[20] F. Baletto and R. Ferrando, Rev. Mod. Phys. **77**, 371 (2005).
[21] Q. Hou, M. Hou, L. Bardotti, B. Prével, P. Mélinon, and A. Perez, Phys. Rev. B **62**, 2825 (2000).
[22] A. V. Granato, Phys. Rev. Lett. **68**, 974 (1992).
[23] K. Nordlund and R. S. Averback, in *Defect and Diffusion in Metals—Annual Retrospective 2000*, edited by D. J. Fisher (Scitec Publications, Zürich, Switzerland, 2000).
[24] R. W. Cahn, Nature (London) **413**, 582 (2001).
[25] M. Forsblom and G. Grimvall, Nat. Mater. **4**, 388 (2005).
[26] F. Delogu, Mater. Sci. Eng., A **403**, 48 (2005).
[27] H. Hertz, J. Reine Angew. Math. **92**, 156 (1881).
[28] U. D. Schwarz, J. Colloid Interface Sci. **261**, 99 (2003).
[29] K. L. Johnson, K. Kendall, and A. D. Roberts, Proc. R. Soc. London, Ser. A **324**, 301 (1971).
[30] H. Zhu and R. S. Averback, Philos. Mag. Lett. **73**, 27 (1996).
[31] Y. Ashkenazy, R. S. Averback, and K. Albe, Phys. Rev. B **64**, 205409 (2001).
[32] W. H. Press, S. A. Teukolsky, W. T. Vetterling, and B. P. Flannery, *Numerical Recipes in C; The Art of Scientific Computing*, 2nd ed. (Cambridge University Press, New York, 1995).
[33] We calculated the energies of the stable and unstable twin boundary positions using a sample of 30 {111} monolayers with a twin boundary in the middle, and conjugate gradient optimization (Ref. 32) to find the minimum-energy configuration. Periodic boundary conditions were applied on the {111} plane. The unstable twin energy was determined by translating the upper half of the system in a $\langle 11\bar{2}\rangle$ direction and calculating the energy again, optimizing the atomic coordinates only in the direction perpendicular to the {111} planes. The energy landscape along this line was determined until a translation of $\frac{a}{\sqrt{6}}$, a being the lattice constant. This slip corresponds to a change in stacking from ⋯AB**C**BA⋯ to ⋯ABC**A**C⋯, that is, the twin boundary (in boldface) moves by one layer. The resulting curve describes the generalized twin fault energy and its highest point gives the unstable twin energy γ_{UTB}.